

# Preliminary Hybrid Joint Analysis for Aircraft Structures

RAUL CORMOS<sup>1,2</sup>, CATALIN ANDREI NEAGOE<sup>2,3</sup>, MIRUNA CIOLCA<sup>2\*</sup>

<sup>1</sup> INCAS - National Institute for Aerospace Research “Elie Carafoli”, 220 Iuliu Maniu Blvd., 061136, Bucharest, Romania

<sup>2</sup> National University of Science and Technology Politehnica Bucharest, Faculty of Industrial Engineering and Robotics, Department Strength of Materials, 313 Splaiul Independentei, 060042, Bucharest, Romania

<sup>3</sup> The Institute of Solid Mechanics of the Romanian Academy, Department of Dynamic Systems, 15 Constantin Mille, 030167, Bucharest, Romania

**Abstract:** *Metal-composite joints, or hybrid joints are prevalent in aerospace structures due to their high strength and low weight. Such structures are usually found in areas where because of the load configuration, the use of composite materials is possible. Thereby, the analysis of such areas needs to consider both components, the metallic and the composite part. In this paper a hybrid joint is analyzed, consisting of a metallic stiffener, a multilayered honeycomb composite material, and joining fasteners, which constitute the joint between the isotropic and orthotropic materials. The present article has two main purposes: the first is to illustrate a pre-design procedure aimed to evaluate the load-carrying capability of a hybrid joint structure, thereby giving an estimate if the structure can withstand the given loading conditions; the second purpose is to present two types of finite element modeling techniques, one that captures the real geometric structure of the composite material and another which uses a simplified equivalent model, based on the desired level of evaluation of the composite material part. A comparison between the two models is made, highlighting the advantages and disadvantages of the two forms of evaluations. For the metallic parts – stiffener and fasteners, both static and fatigue analyses were performed, as fatigue failure represents the common service failure mode for this type of structural components.*

**Keywords:** *hybrid joint, honeycomb composite, finite element analysis, fatigue analysis, Nastran, VBA*

## 1. Introduction

Composite and metal joints, often named hybrid joints, are commonly used in the aerospace industry, where weight saving, and high strength is necessary [1-3]. These joints are made of three main components: a metallic part, a composite part and joining elements set between the metallic and composite materials. Usually, metallic fasteners are used in aerospace applications, to obtain a more ductile behavior.

The failure of any of these components in a hybrid joint automatically leads to the failure of the entire assembly. Thereby, a thorough analysis is required to make sure that such assemblies do not fail under structural loading. In the aerospace industry, such joints are used for example, for wings or fuselage parts, where the outer skin is made of a composite material, and a local stiffener is required. A typical hybrid joint for an aircraft skin is presented in Figure 1.

The considered composite joint is made of honeycomb composite material, usually subjected to aerodynamic pressure resulting from the fluid flow around the aircraft. Aerodynamic loads are frequently turbulent in nature and are dependent on many factors, not just the aircraft speed, but also on weather conditions, a fact which causes such loads to be non-stationary – as a result, a complex analysis is required for this type of structural components. The metallic part, in this case, has the main role to act as a local stiffener, adding additional stability, and to transfer loads to the main structure.

The behavior of metal-composite joints under static or dynamic loads, the performance and failure modes have been investigated both experimentally and numerically [4-6]. These studies have shown that, in order to analyze the mechanical behavior of the structural components, the complete spatial modeling of the composite part is not quite an acceptable solution due to the very high number of degrees

\*email: [miruna.ciolca@upb.ro](mailto:miruna.ciolca@upb.ro)

of freedom of the finite element model, and therefore, these type of detailed modeling techniques are preferred instead for local phenomena analyses. Consequently, a simplified numerical model that would be able to capture the structural performance of an intricate hybrid joint would be desired for faster analysis and design procedures.

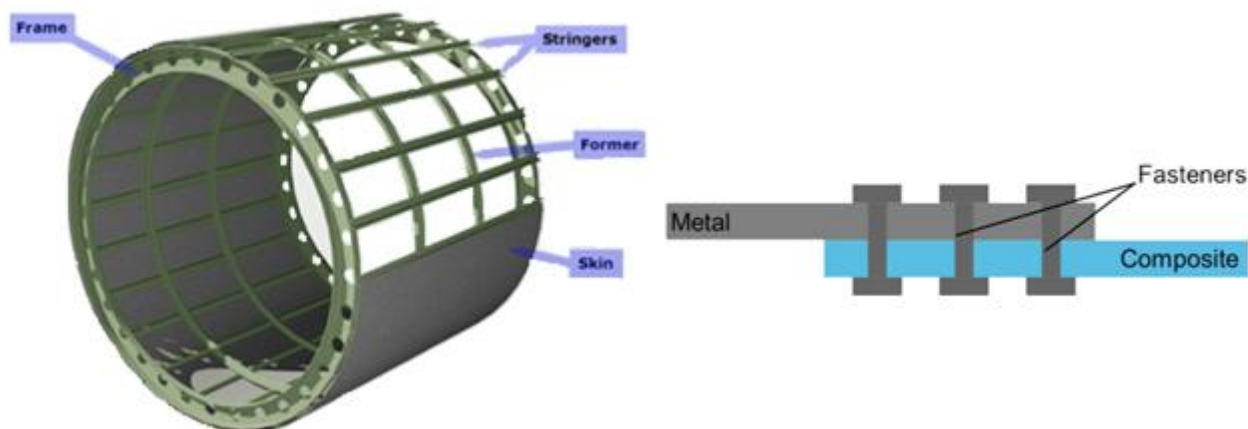


**Figure 1.** Aircraft structure [7] and hybrid joint example [8]

In addition, for metallic structural components used in aerospace vehicles, fatigue failure represents the most common service failure mode [9]. Fatigue failure embodies an important area of study due to its prevalent and hard to analyze nature [10,11]. These characteristics are given by the nature of repetitive loading and the parameters required to accurately predict fatigue failure. It is very important to carry out a fatigue analysis especially on primary structural components whose failure can lead to catastrophic results, even in the service period of highly complex mechanical structures.

In this paper, a reduction of the complexity of the multilayer honeycomb composite material has been investigated by using the equivalent mathematical model given by Gibson [12], for the honeycomb core, and a local preliminary comparative analysis is performed between the two distinct forms of composite modeling. The two forms are represented by: a multilayered model, highlighting the spatial geometry of all the layers, and a single layer model, considering only one effective layer for the whole composite material, for a simplified analysis. With respect to the non-stationary behavior of aerodynamic loads, both static and fatigue evaluations have been performed – the latter only for the metallic parts – to assess the structural load carrying capacity for the given load case and the estimated lifespan under cyclic loading.

## 2. Materials and methods

### 2.1. Assembly description

The structure analyzed in this paper is a part of an aircraft fuselage. Its components and geometry are similar to the ones used in aircraft skin manufacturing.

The assembly consists of a square multilayered honeycomb composite material that is bolted on top of a T-shaped metallic stringer, which has the role to transfer outside loads to the frames and ensure rigidity. Figure 2 illustrates the geometry and dimensions of the structural assembly and its parts.

The multilayered honeycomb composite material is made up of five layers of materials, totaling 15 mm in height. The layers consist of two double-layered composite sheets made of woven fiber glass (1.17 mm each), forming the outer faces of the composite part; and two Nomex honeycomb paper cores (6 mm each) impregnated with polyester resin and separated by a single layer sheet (0.65 mm) of the same material as the outer faces. The two paper cores overlap in configuration and have a network of slightly elongated hexagonal shapes, aligned in the crosswise direction of the stiffener.

The composite part is fixed to the top flange of the metallic part, on each side, with four titanium alloy bolts that have a diameter of 4 mm, placed at a distance of 16 mm from the edges. The T-shaped stringer is made of an aluminum alloy and has a thickness of 2 mm.

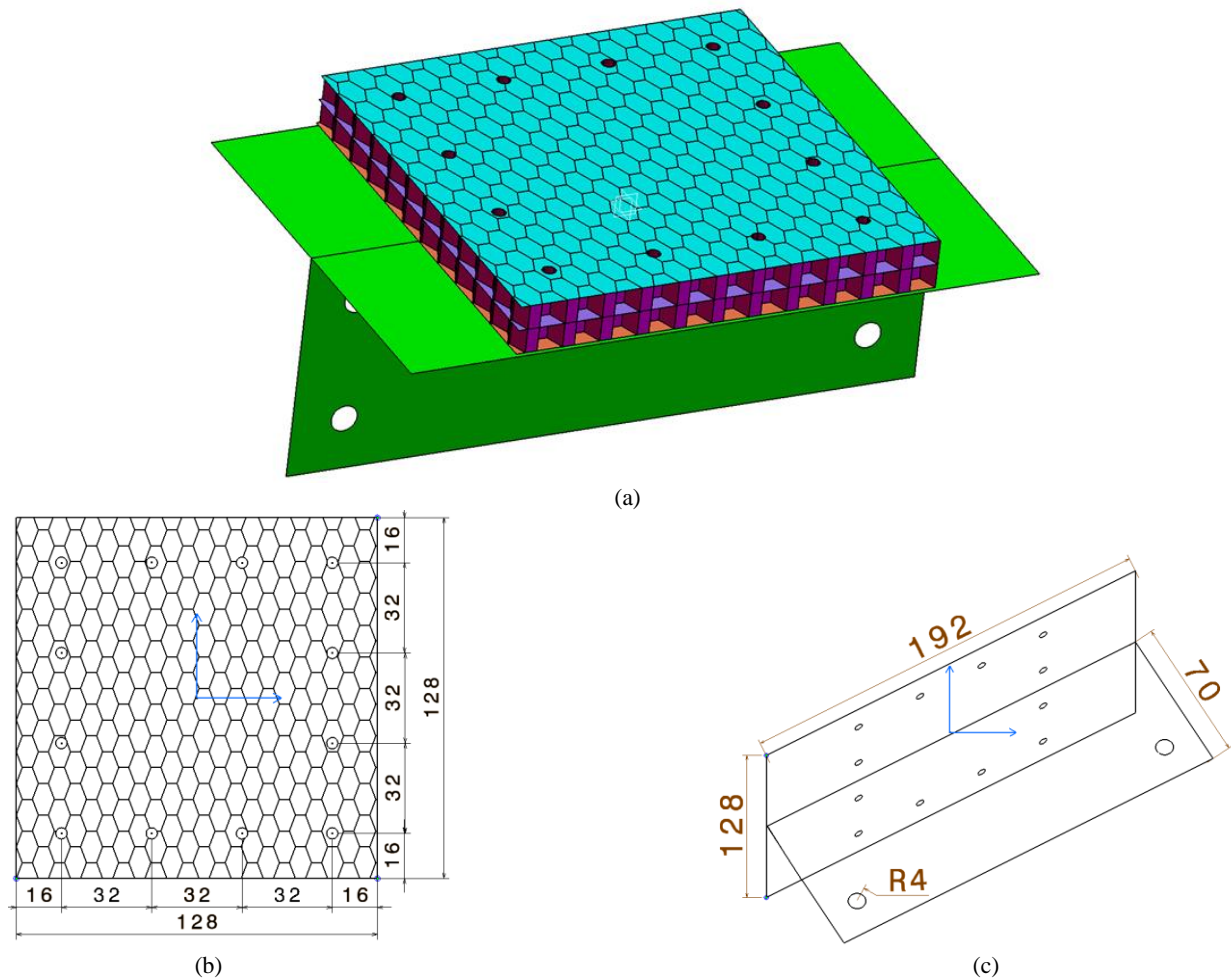


**Figure 2.** Assembly geometry and dimensions: (a) assembly geometry – multilayered composite model (MSC Nastran); (b) honeycomb dimensions and fastener hole positions; (c) metallic stiffener dimensions

## 2.2. Material properties

To begin with, the mechanical properties for the metallic parts of the analyzed hybrid joint are provided in Table 1.

**Table 1.** Mechanical properties of metallic components [13]

Part	Material	Elastic modulus [MPa]	Poisson's ratio
Stiffener	Al	71,000	0.33
Fasteners	Ti	116,500	0.31

The mechanical properties for the composite glass fiber sheets and honeycomb paper cores are presented in Table 2 and Table 3. These material data were determined experimentally, by laboratory testing, and reported by the first author in [14].

**Table 2.** Mechanical properties of the woven glass fiber sheets [14]

Material property	Characteristic	Value	Unit of measurement
Elastic moduli	$E_x$	16,954	[MPa]
	$E_y$	14,684	[MPa]
	$E_z$	7,122.9	[MPa]
Poisson's ratios	$\nu_{xy}$	0.129	
	$\nu_{yz}$	0.109	
	$\nu_{zx}$	0.33	
Shear moduli	$G_{xy}$	5,942.3	[MPa]
	$G_{yz}$	5,014.3	[MPa]
	$G_{zx}$	3,138.5	[MPa]

**Table 3.** Material data for the impregnated Nomex paper core [14]

Elastic modulus [MPa]	Poisson's ratio	Shear modulus [MPa]
16,357	0.35	6058.15

To construct the single layer model for the whole composite part, to serve in the simplified analysis, an equivalent orthotropic material was considered for the honeycomb cores. The mathematical model used to compute the elastic properties of the cores [12,15,16] is presented below, and the explicit geometric data of the honeycomb cores, used in the mathematical expressions, are indicated in Figure 3 – where  $t$  represents the cell's thickness,  $l$  the length of the inclined cell walls,  $h$  the length of the cell's side walls, and  $\theta$  the angle of the inclined cell wall.

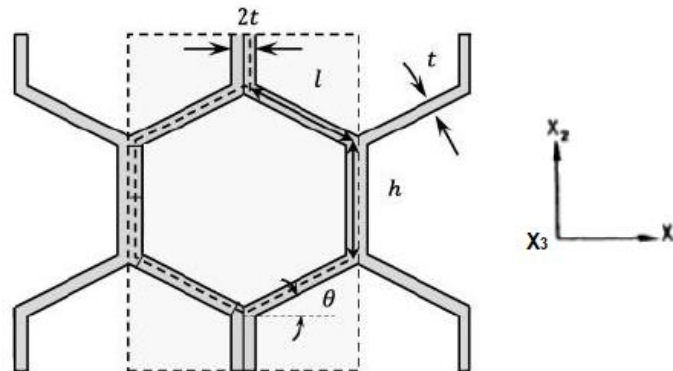


**Figure 3.** Honeycomb cell geometric data – adapted from [12]

1. Transverse elastic modulus for the cell wall:

$$G = \frac{E}{2 \cdot (1 + \nu)} \quad (1)$$

where:

$E$  – material's longitudinal elastic modulus;  
 $\nu$  – Poisson's ratio.

2. Modulus of elasticity of orthotropic honeycomb core on  $X_1$  direction:

$$E'_1 = E \cdot \left(\frac{t}{l}\right)^3 \cdot \frac{\cos(\theta)}{\left(\frac{h}{l} + \sin(\theta)\right) \cdot \sin^2(\theta)} \quad (2)$$

3. Modulus of elasticity of orthotropic honeycomb core on  $X_2$  direction:

$$E'_2 = E \cdot \left(\frac{t}{l}\right)^3 \cdot \frac{\left(\frac{h}{l} + \sin(\theta)\right)}{\cos^3(\theta)} \quad (3)$$

4. In-plane Poisson's ratio:

$$\nu'_{12} = (\nu'_{21})^{-1} = \frac{\cos^2(\theta)}{\left(\frac{h}{l} + \sin(\theta)\right) \cdot \sin(\theta)} \quad (4)$$

5. Transverse shear modulus on  $X_1$ - $X_2$  plane:

$$G'_{12} = E \cdot \left(\frac{t}{l}\right)^3 \cdot \frac{\left(\frac{h}{l} + \sin(\theta)\right)}{\left(\frac{h}{l}\right)^3 \cdot \left(1 + \frac{h}{4l}\right) \cdot \cos(\theta)} \quad (5)$$

6. Elastic modulus in out-of-plane direction:

$$E'_3 = E \cdot \left(\frac{t}{l}\right) \cdot \frac{\left(\frac{h}{l} + 1\right)}{\cos(\theta) \cdot \left(\frac{h}{l} + \sin(\theta)\right)} \quad (6)$$

7. Out-of-plane Poisson's ratios:

$$\nu'_{23} = \nu'_{13} = \nu \quad (7)$$

8. Transverse shear modulus on  $X_1$ - $X_3$  plane:

$$G'_{13} = G \cdot \left(\frac{t}{l}\right) \cdot \frac{\cos(\theta)}{\left(\frac{h}{l} + \sin^2(\theta)\right)} \quad (8)$$

9. Transverse shear modulus on  $X_2$ - $X_3$  plane:

$$G_{23}^{inf} \geq G \cdot \left(\frac{t}{l}\right) \cdot \left(\frac{\frac{h}{l} + \sin(\theta)}{\left(\frac{h}{l} + 1\right) \cdot \cos(\theta)}\right) \quad (9)$$

$$G_{23}^{sup} \leq G \cdot \left(\frac{t}{l}\right) \cdot \left(\frac{\frac{h}{l} + \sin^2(\theta)}{\left(\frac{h}{l} + \sin(\theta)\right) \cdot \cos(\theta)}\right) \quad (10)$$

$$G'_{23} = G_{23}^{inf} + \frac{0.787}{\frac{h}{l}} \cdot (G_{23}^{sup} - G_{23}^{inf}) \quad (11)$$









Considering that the honeycomb's cell  $\theta$  angle is  $20^\circ$ , the following results were calculated and introduced in the simplified finite element model for the equivalent orthotropic material. These elastic properties are presented in Table 4.



**Table 4.** Equivalent orthotropic material data for the honeycomb cores

$E'_1$ [MPa]	$E'_2$ [MPa]	$\nu'_{12}$	$\nu'_{21}$	$G'_{12}$ [MPa]	$E'_3$ [MPa]	$\nu'_{23}=\nu'_{13}$	$G'_{13}$ [MPa]	$G'_{23}$ [MPa]
7.86	1.05	2.74	0.36	2.23	1133.32	0.35	231.66	201.37

The lay-up of the single layer composite model is presented in Figure 4. The stacking direction is vertical.

Ply lay-up:		Composit figure			
Total number of plies: 5					
Total thickness: 14.99					
		Ply	Material	Thickness T1	Orientation Degrees
		1	Composit	1.17	0.0
		2	Fagure_ortotrop	6.0	0.0
		3	Composit	0.65	0.0
		4	Fagure_ortotrop	6.0	0.0
		5	Composit	1.17	0.0

**Figure 4.** Single layered composite lay-up

### 2.3. Finite element models

Two finite element models were created, one for each of the two composite material configurations. The first model is a complex multilayered spatial representation of the composite material while the second one is a plane, single layer equivalent model of the composite material. For the finite element analyses, the MSC Nastran solver was used [17].

In both finite element models, the structure has three components: the metallic part, with the element size of 1.4 mm, the composite part with a 0.4 mm element size, and the fastener joints between them that are modeled with beam elements (CBAR). The multilayered composite material model contains a total number of 828,641 elements and 797,210 nodes, while the single layer model, with only one row of shell elements, contains a total number of 226,050 elements and 227,597 nodes, on which all five layers are defined. All 2D element types are first order plate elements (CTRIA3 and CQUAD4). The two finite element models are presented in Figure 5.

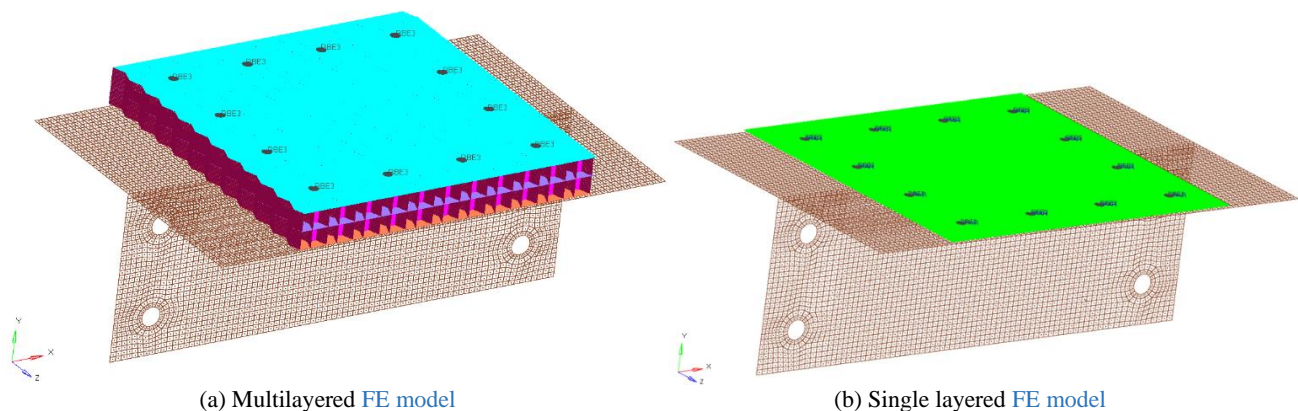


**Figure 5.** Finite element models for: (a) multilayered composite structure;  
(b) single layer composite structure

The connection between the main components is assured using RBE3 type rigid elements around the holes, linked with CBAR elements on the middle nodes, in order to constraint and distribute forces around the connected nodes, for the simulated metallic fasteners.

For the material orientation of the composite layers, the global longitudinal X axis direction is considered. The element normal direction for the composite layers is the positive direction of the global vertical Y axis. This is important to specify, because this direction defines the stacking order of the composite layers and, later, the load application direction.

## 2.4. Boundary and loading conditions

For the boundary conditions, two single point constraints (SPCs) were defined on the metallic stiffener: one support with all translational degrees of freedom blocked (components 1,2,3), on the edges of the metallic part, so as not to introduce reaction moments, and a second support with all degrees of freedom blocked (components 1,2,3,4,5,6) on the lower four holes of the metallic part. Figure 6 shows the constraints used in the finite element analyses.

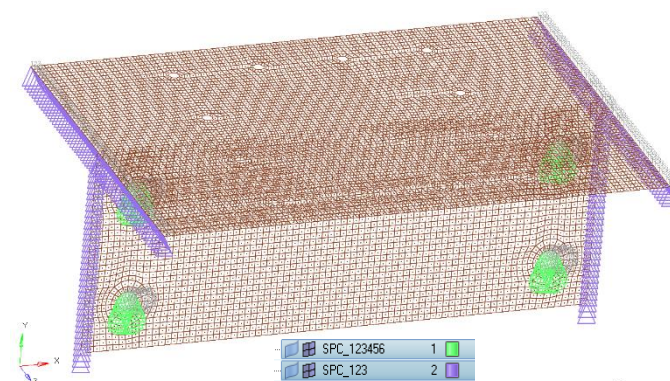


**Figure 6.** Boundary conditions set for the finite element models

Loading was introduced by applying pressure, using the PLOAD2 Nastran card, simulating a 2000 N distributed load over the top composite material area. The resulting compressive pressure value is equal to -0.124 MPa. The minus sign indicates that the loading direction is in the opposite direction of the global vertical Y axis. This pressure load was applied on the upper sheet of the multilayered composite model or on top face of the single layer composite model. The loading scheme presented in Figure 7, subjects the entire structural assembly to bending.

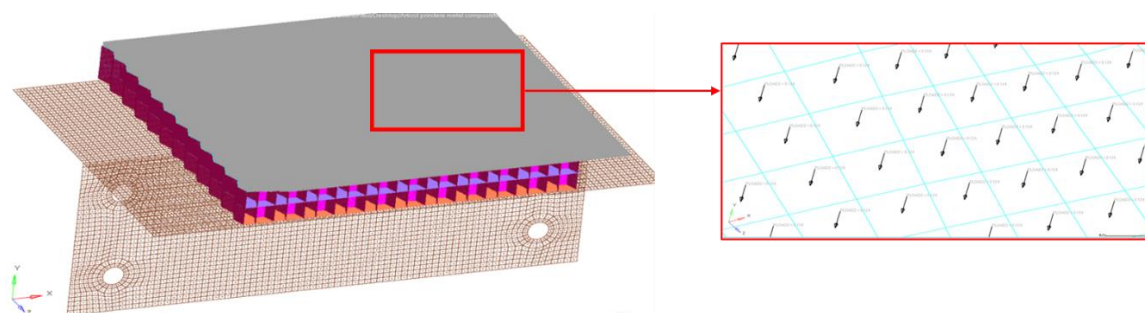


**Figure 7.** Pressure load application on finite element model and loading direction

## 2.5. Results evaluation methods

To evaluate and compare the results from the two finite element models, the following evaluation methods are used for each of the structural components.

For the woven glass fiber composite sheets (layers 1, 3 and 5), the minimum principal strain, corresponding to the maximum achieved value for the compressive stress is presented. This value can

be regarded as a measure of the woven composite layers' loading level, in correspondence with the maximum strain failure criterium for laminated composite materials [18-20].

For the honeycomb paper cores (layers 2 and 4), the maximum displacements are shown. This parameter's value represents a reasonable measure to evaluate the loading state of the honeycomb cores. Thus, if the displacement is relatively small in comparison to the core's height, it can be considered that the core is not loaded with a force that would justify other evaluation criteria for it. Studies have shown that failure can occur for a 5-10% value of the compressive strain and for similar percentages in relative vertical displacement for cores [21, 22].

In the case of the metallic parts from the hybrid joint, it is possible to do not just a static, but also a fatigue behavior evaluation, given the material properties. The fatigue behavior is useful to be considered if the nature of the loading is non-stationary and the service life of the components are evaluated.

For the fasteners, a static evaluation was performed using the resulting forces on tension and shear components, by comparing these values with the static allowable computed values. For the fatigue behavior, a symmetrical alternating load cycle was considered, and the maximum stress amplitude was calculated. The maximum numbers of load cycles were estimated using the Wohler curve of the material considered for the fasteners.

In the case of the metallic stiffener, the static evaluation consisted in comparing the maximum predicted von Mises stress to the indicated yield strength of the material. For the fatigue behavior investigation, a pulsating load cycle was considered as being more dangerous for the structural assembly, and the maximum principal stress was computed. From it, the stress amplitude was calculated, thereby allowing, by using Wohler curve, to estimate the number of cycles that the stiffener can withstand.

The mathematical models used for the evaluations of the metallic parts are presented together with the results.

The results were calculated using MSC Patran software, on element centroid extrapolation, meaning that the values were obtained in the element center and not averaged on nodal results. The results were extracted from selected central areas on the composite part, avoiding stress concentrator effects caused by holes, and poor-quality elements resulting from the proximity of hard modeling areas.

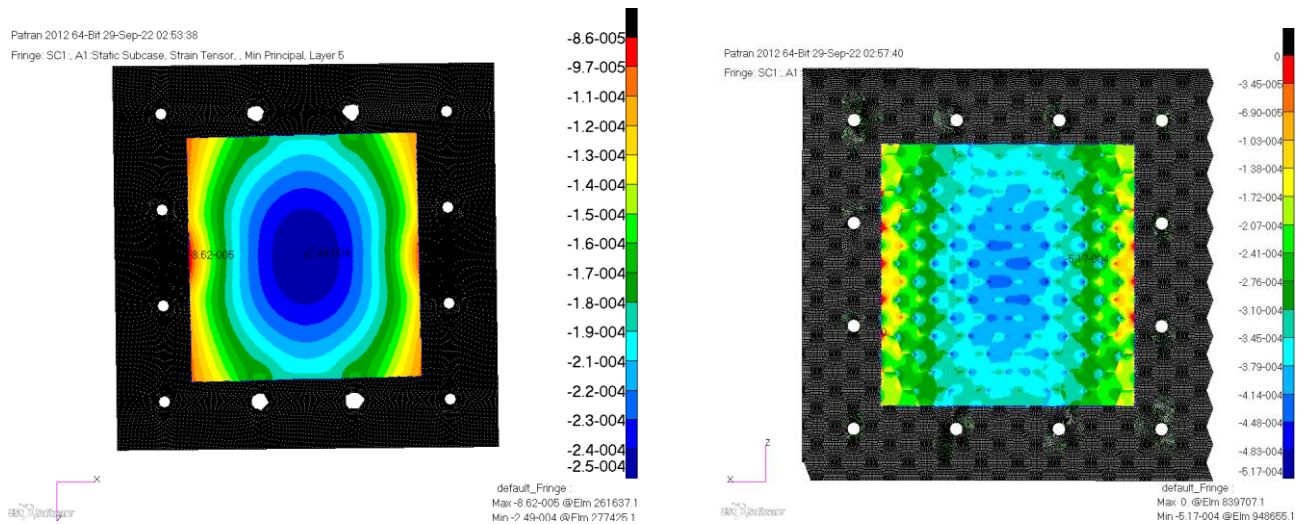
### 3. Results and discussions

After completing the preliminary analyses, the obtained results can be further used to assess the hybrid structure's load carrying capacity and to evaluate if it can withstand a given load case scenario. The initial results are presented in a comparative manner, on both developed finite element models – single and multilayered. The evaluations were carried out individually, for each constitutive part of the assembly. Because in the case of the composite materials, the ultimate strain was not determined experimentally, the following results are more characteristic of the static behavior and do not capture the failure modes. Besides the static simulations, for the metallic parts – stiffener and fasteners, the non-stationary fatigue load behavior is also considered in the analyses.

#### 3.1. Composite woven sheets analysis

The composite woven sheets – top, middle, and bottom layers (layers 5, 3 and 1) were analyzed considering the minimum strain criteria, given the fact that the composite material was subjected to a compressive load. To avoid stress concentrator effects around the fastener holes, the strain distributions were plotted for the central area of the composite layers [23].

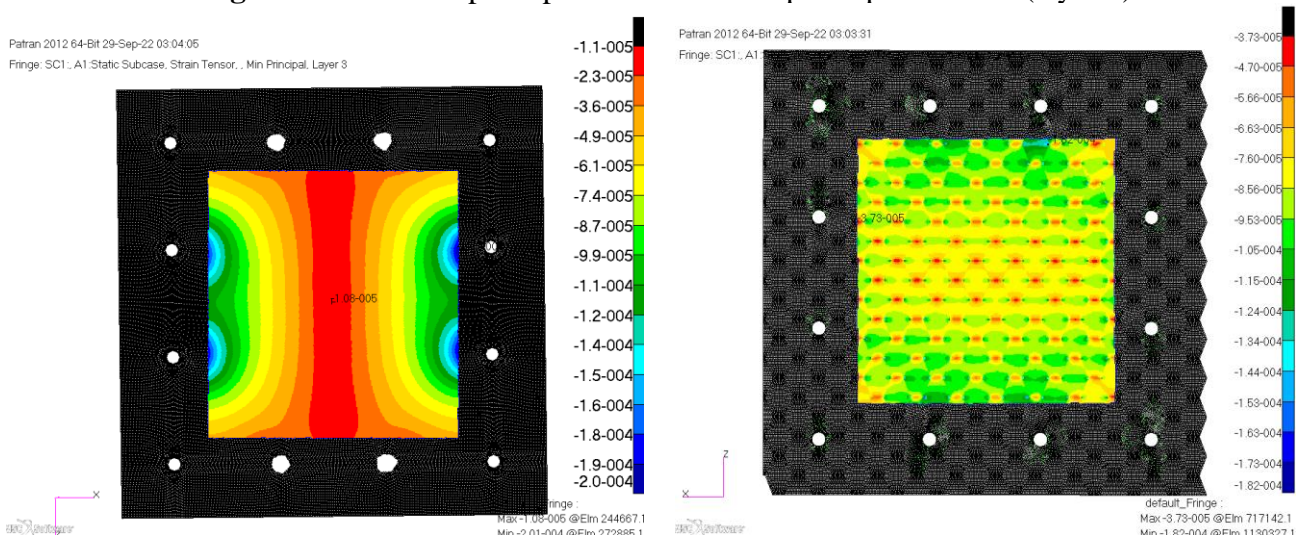




(a) Single layered model:  $-2.50 \times 10^{-4}$  mm/mm

(b) Multilayered model:  $-4.18 \times 10^{-4}$  mm/mm

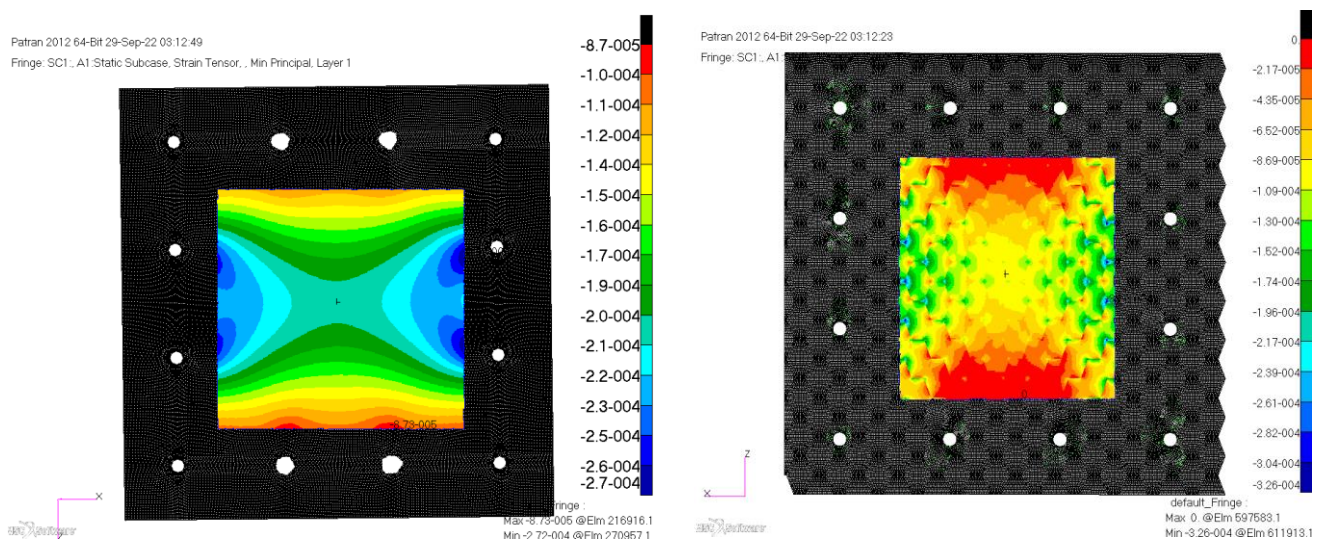
**Figure 8.** Minimum principal strain for the top composite sheet (layer 5)



(a) Single layered model:  $-2.00 \times 10^{-4}$  mm/mm

(b) Multilayered model:  $-1.82 \times 10^{-4}$  mm/mm

**Figure 9.** Minimum principal strain for the middle composite sheet (layer 3)



(a) Single layered model:  $-2.70 \times 10^{-4}$  mm/mm

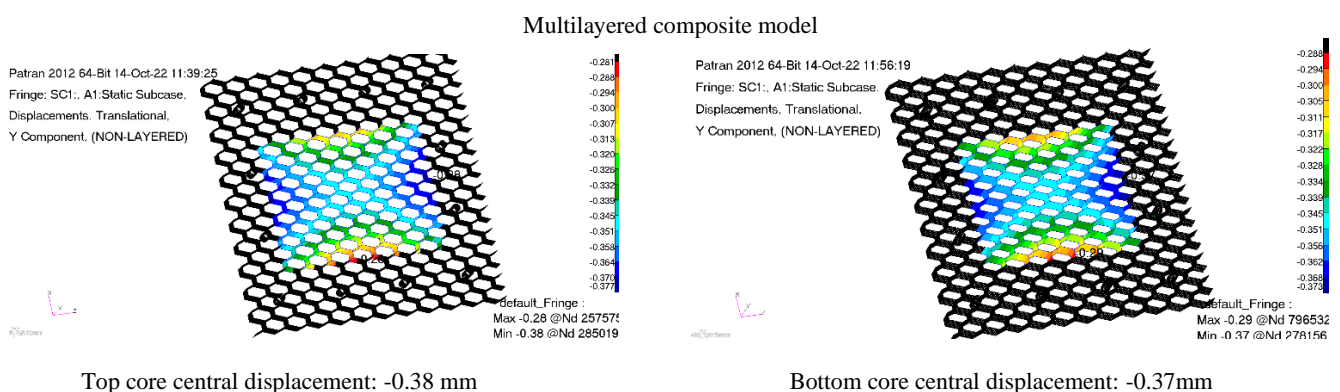
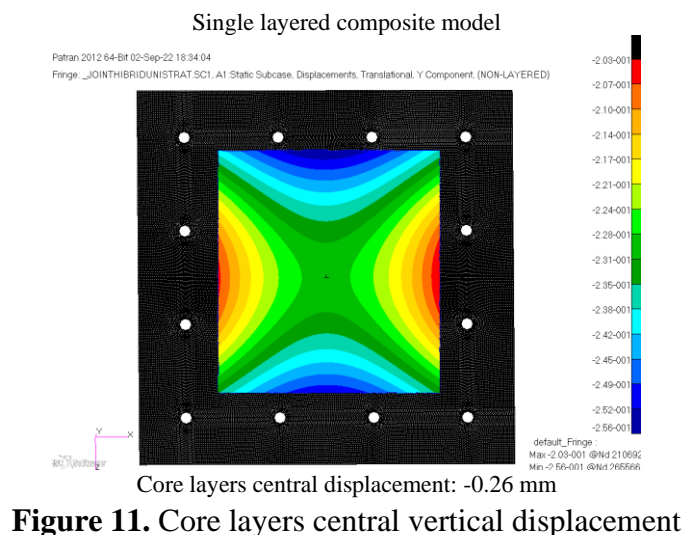
(b) Multilayered model:  $-3.26 \times 10^{-4}$  mm/mm

**Figure 10.** Minimum principal strain for the bottom composite sheet (layer 1)

Figures 8, 9 and 10 display the minimum principal strain values for the three glass fiber sheets, on both finite element models. The strain values are negative because the minimum principal strain was considered for evaluation. These values correspond to the maximum compressive stress, equivalent to the highest compression deformation. The variation of the strain presented above, on each layer, is caused by the bending moment variation along the total thickness of the composite material, on both the X and Z axis. In the multilayered composite structure, the woven sheets have the role to take the in-plane stress corresponding to the X-Z plane.

### 3.2. Honeycomb core displacement evaluation

A similar procedure is followed for the honeycomb cores (layers 2 and 4), the difference is that the maximum displacement on the global Y vertical axis is analyzed. In this case, the cores act as a flexural stiffener for the composite material, loaded in compression along the Y axis. Because the maximum and minimum strain criteria are specific for layered composites, the small deformations of the core were evaluated. Hence, if the core deformation is small related to its height, it can be considered that no significant compressive stress is registered, and the core can safely take the compressive load. Therefore, this method constitutes a preliminary way to evaluate the core's behavior, as seen in Figure 11 and Figure 12.



The obtained central core displacements for the multilayered composite model are slightly larger compared to the one obtained in the simplified equivalent model. Even so, the values are sufficiently small compared to the cores' total height of 12 mm, thereby confirming that the core can withstand the given load.

### 3.3. Fastener analyses

The fasteners on the 12 holes which constitute the joint between the composite and the metal stringer are analyzed only from the point of view of the joining elements between them. For these analyses, conventional strength of material and machine element theory has been employed [24, 25].

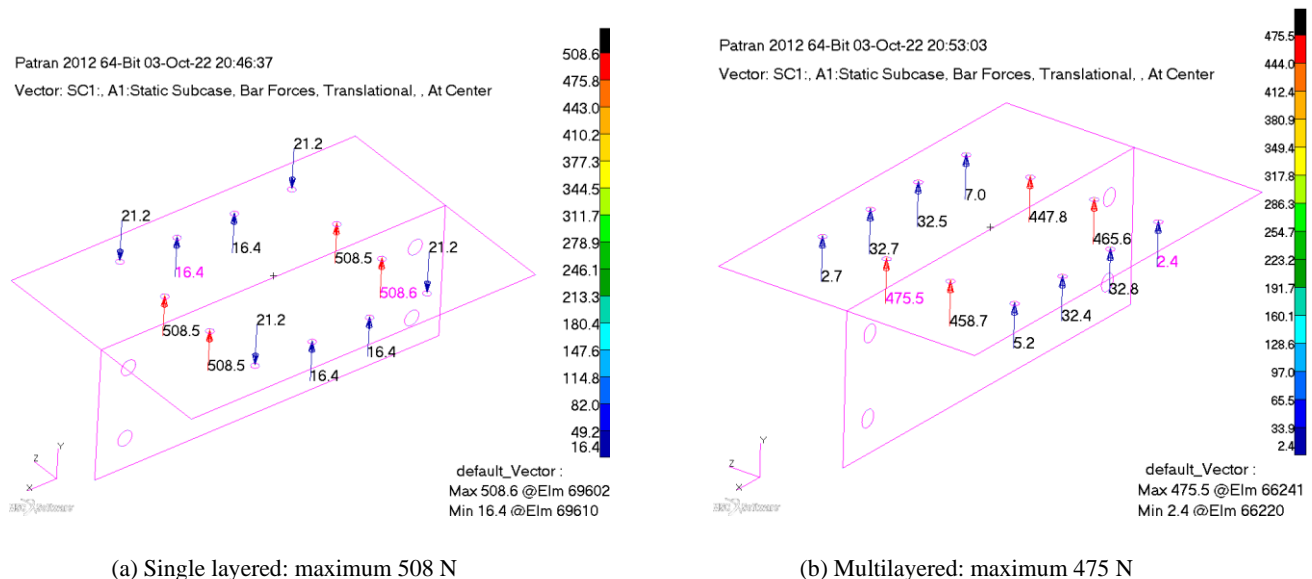
#### 3.3.1. Fastener static analysis

Considering the fasteners' geometric data and the ultimate strength values of the employed material, the shear and the axial capacity values were computed. For a typical titanium alloy, the ultimate strength value can be considered  $\sigma_u = 880$  MPa [13]. The ultimate shear strength is, therefore:  $\tau_u = 0.6 \cdot \sigma_u = 528$  MPa. Considering that the diameter  $D$  of the connectors is 4 mm, the admissible axial and shear force capacities were calculated ( $F_{tu}$  and  $F_{su}$ ). Usually, for commercial fasteners, this information is provided by manufacturers, according to the standards used in production.

$$F_{tu} = \sigma_u \cdot \pi \cdot \frac{D^2}{4} = 11058 \text{ N} \quad (12)$$

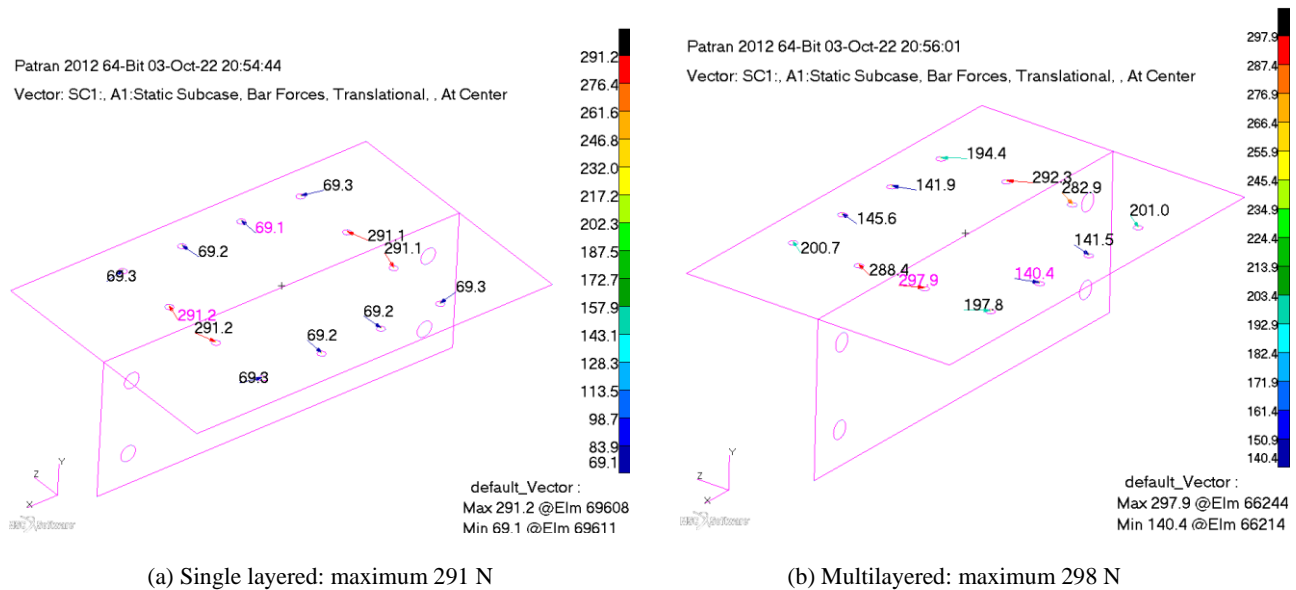
$$F_{su} = \sigma_u \cdot 0.6 \cdot \pi \cdot \frac{D^2}{4} = 6635 \text{ N} \quad (13)$$

Figure 13 and Figure 14 show the maximum axial and shear forces that occur in the hybrid joint's fasteners, calculated for both FE models, under the applied load case scenario.



**Figure 13.** Estimated axial forces in the fasteners





**Figure 14.** Estimated shear forces in the fasteners

For both models, the maximum predicted shear and axial forces are below the considered allowable values.

### 3.3.2. Fastener fatigue evaluation

Since the external loads can be caused by non-stationary phenomena, a fatigue analysis is recommended to be carried out. For a preliminary evaluation of the fasteners' lifespan expectancy, the fatigue loading can be considered equivalent to a static loading repeated several times, equivalent with the number of cycles that the part is in use.

To perform the fatigue analysis, a Wohler curve is considered for the titanium alloy [13], as shown in Figure 15.

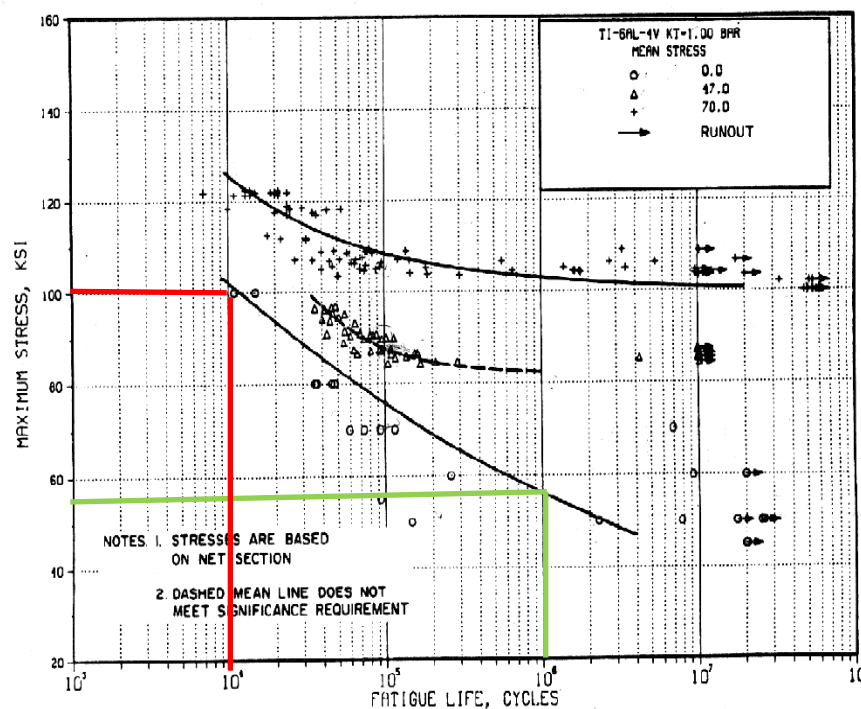


**Figure 15.** Wohler curve for a typical titanium alloy [13]

The mathematical model used for the computation of the fatigue analysis has been presented in [26-30]. The fatigue curve equation has been solved for two points on the Wohler curve:

$$\sigma_a = \sigma_f' \cdot (2 \cdot N_f)^{1/b} \quad (14)$$

where:

- $\sigma_a$  – stress amplitude;
- $\sigma_f'$  – stress curve constant;
- $N_f$  – number of cycles to failure;
- $b$  – Wohler curve constant.

Considering two points on the Wohler curve, illustrated by the red and green lines in Figure 15, for a stress amplitude and an allowable number of cycles ( $10^4$  and  $10^6$ ), it is possible to compute  $\sigma_f' = 2218$  MPa and  $b = -0.118$ , and thus the Wohler curve equation can be constructed.

To carry out the fatigue evaluation, the maximum von Misses stress was considered. The stress amplitude in the fatigue load cycle was considered as half of the respective von Misses stress. The last was calculated using the following relation:

$$\sigma_{VM} = \sqrt{\sigma^2 + 4 \cdot \tau^2} \quad (15)$$

where:

- $\sigma$  – axial stress;
- $\tau$  – tangential stress;
- $F_t$  – axial force;
- $F_{sh}$  – shear force.

Table 5 shows the results obtained from the fastener fatigue analysis.

**Table 5.** Fastener fatigue analysis results

Composite model	$F_t$ [N]	$F_{sh}$ [N]	$D$ [mm]	Area [mm <sup>2</sup> ]	$\sigma$ [MPa]	$\tau$ [MPa]	$\sigma_{VM}$ [MPa]	$\sigma_a$ [MPa]	$\sigma_a$ [ksi]
Multilayer	474	298	4.0	12.6	37.7	23.7	60.6	30.3	4.4
Single layer	508	291	4.0	12.6	40.4	23.2	61.5	30.7	4.5

The stress amplitude is below the infinite stress amplitude in the Wohler curve, thereby it can be said that for the given load case, the fasteners have a theoretically infinite life. Comparing the results in terms of stresses or forces, the observed differences are relatively small. This suggests that the composite part modeling technique and the introduced load on the composite model have a limited influence on the forces or stresses maximum values.

### 3.4. Stiffener analyses

#### 3.4.1. Stiffener static analysis

To evaluate the stress levels on the metallic stiffener, a yield strength of 520 MPa [13] was considered for the aluminum alloy. The resulting von Misses stress is compared with the maximum value for both models. The stress results are shown in Figure 16.



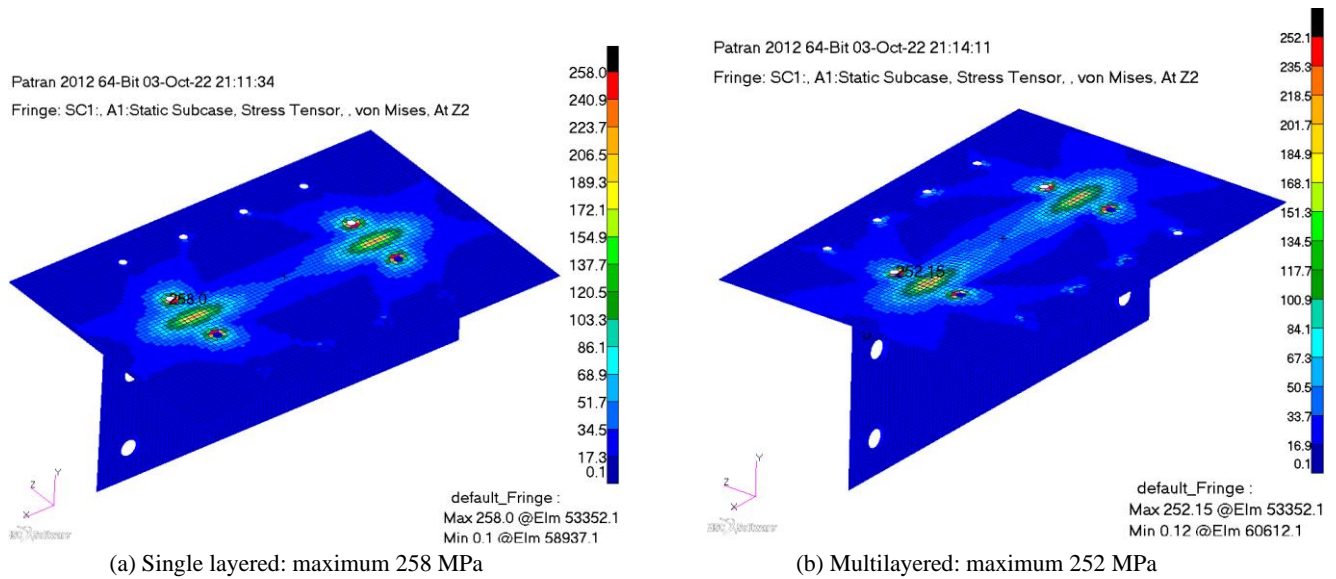


**Figure 16.** Maximum von Mises stress values for the two FE models

Even considering the stress concentrator areas around the fastener holes, the effective stress values are below the yield strength of the material. The von Mises stress on both models has an almost identical value, leading to the conclusion that the stresses registered on the stiffener have no dependency on the model type, single or multiple layer composite structure.

### 3.4.2. Stiffener fatigue evaluation

To evaluate the fatigue behavior of the stiffener, a similar mathematical model was used for the fasteners, with the difference that in this case, the maximum and minimum principal stress were taken into consideration. By eliminating the stress concentrator areas around the holes and plotting the maximum and minimum principal stresses, the following results displayed in Figure 17 and Figure 18 were obtained.

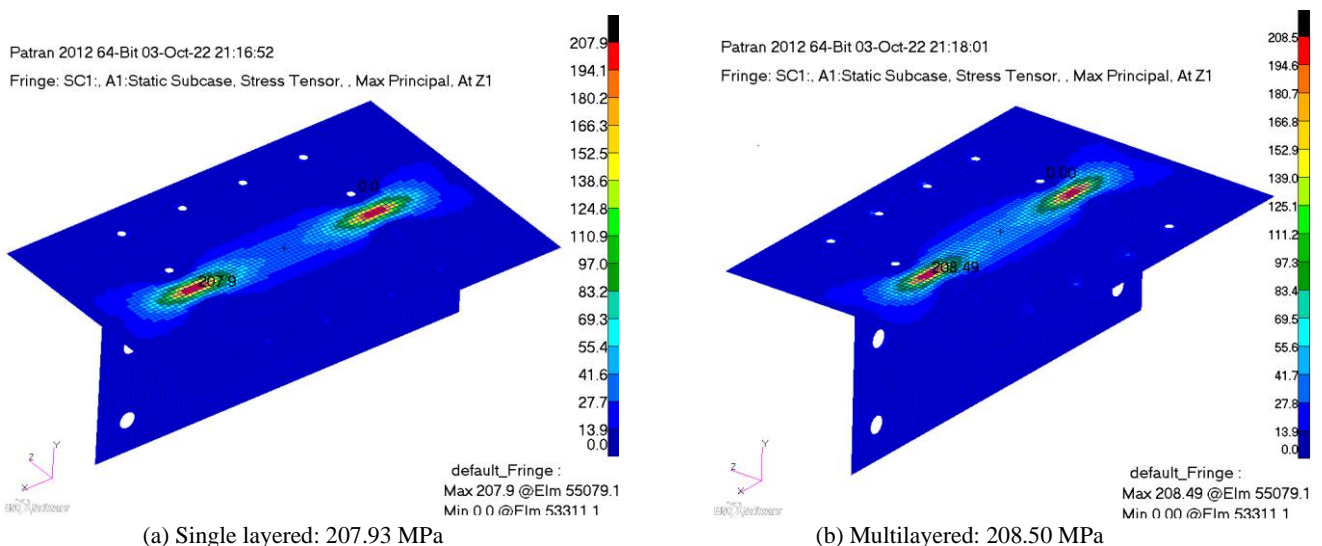


**Figure 17.** Maximum principal stress on metallic stiffener

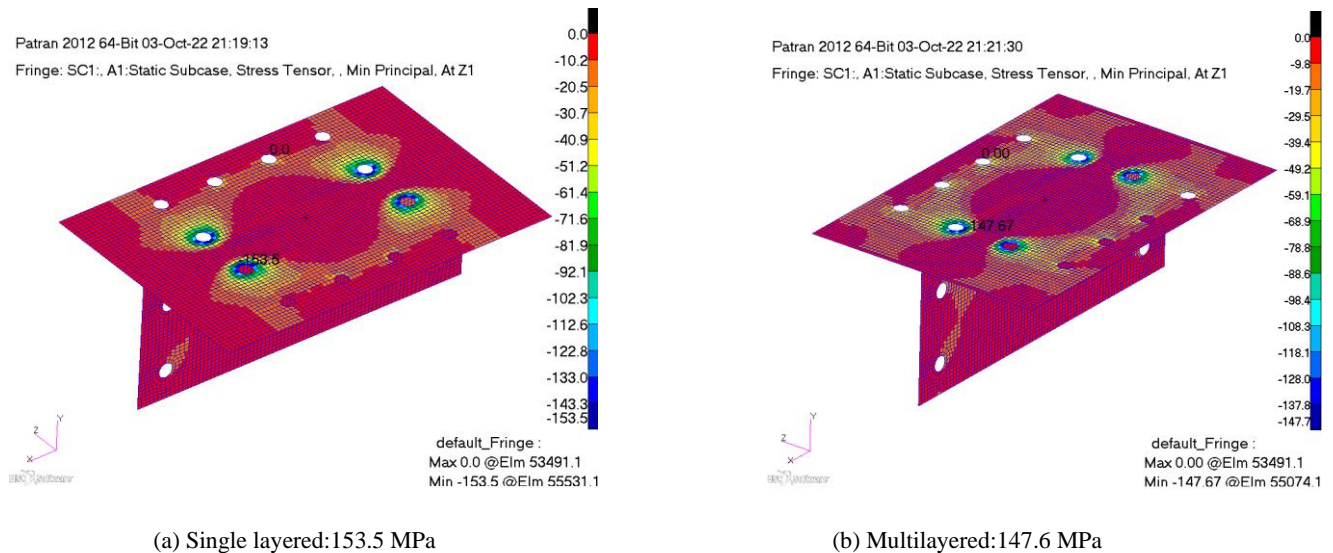


**Figure 18.** Minimum principal stress on metallic stiffener

From the comparison of the maximum and minimum stress plots of the two models it can be observed that both stresses appear in the same area and have close values, indicating the same conclusion as of the static evaluation case.

To advance this analysis, an aluminum alloy fatigue curve was chosen, illustrated in Figure 19.

As a less conservative hypothesis, the upper fatigue curve was chosen for the allowable lifespan evaluation.

Two points were chosen to compute the 2 terms for the stress amplitude-lifespan. These points were marked on the figure as  $P_1$  (70 ksi/482 MPa, 11,000 cycles) and  $P_2$  (27 ksi/186.16 MPa,  $10^7$  cycles). The computed values for the fatigue curve equation are  $b = -0.137$  and  $\sigma'_f = 1934$  MPa.

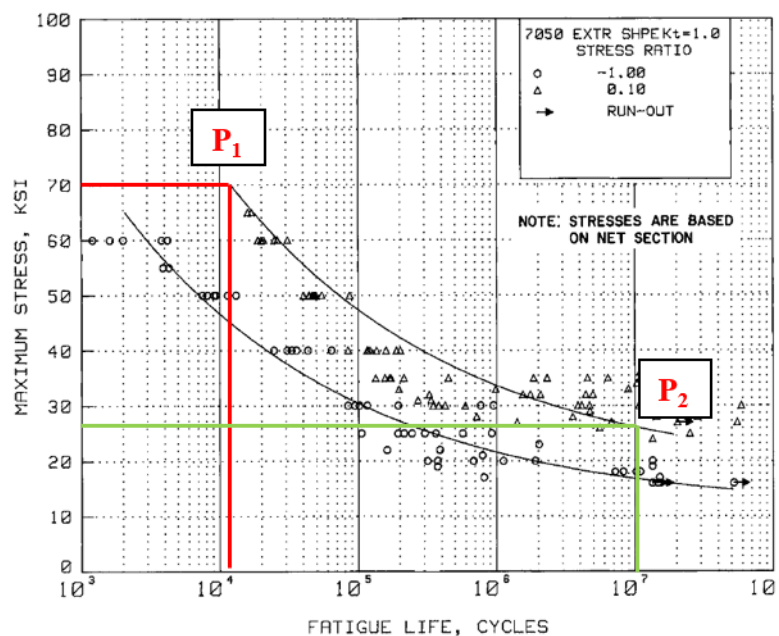


**Figure 19.** Wohler curve for Al 7050 [13]

The stress amplitude  $\sigma_a$  and the mean stress  $\sigma_m$  were computed using the formulas:

$$\sigma_a = \frac{\sigma_{max} - \sigma_{min}}{2} \quad (16)$$

$$\sigma_m = \frac{\sigma_{max} + \sigma_{min}}{2} \quad (17)$$

where:

$\sigma_{max}$  – maximum principal stress;

$\sigma_{min}$  – minimum principal stress.

To correct the values for non-zero mean stress, the Gerber correction has been used:

$$\sigma_{ac} = \frac{\sigma_a}{1 + \frac{\sigma_m}{\sigma_f}} \quad (18)$$

where:

$\sigma_{ac}$  – Gerber correction stress amplitude.

A mean stress correction is used to change a general stress cycle to a corresponding stress cycle with zero mean stress. Using the Gerber corrected amplitude [13], the allowable numbers of cycles for which the stiffener can be used is calculated using the computed Wohler curve equation.

After completing the computations for the single layered composite model, the maximum Gerber corrected stress amplitude is 100 MPa, corresponding with a very high allowable number of cycles in use. For the multilayered composite model, the corrected stress amplitude is 85.6 MPa. To consider the stress concentrator effects, the 100 MPa value is multiplied with 3, and this stress amplitude of 300 MPa offers an allowable life expectancy of 349,000 cycles. For the single layered model, a specially written program for comparative evaluation was made in VBA. The results were similar, considering the stress concentrator, and the allowable number of cycles obtained was 304,000 cycles.

These prediction values are for a predesign concept. For a final detailed analysis, all failure criteria should be considered, but for such high values and for the given load case scenario, on a preliminary evaluation, the intended structure can withstand the given load case.

## 4. Conclusions

The current study presented a pre-design procedure aimed to evaluate the load-carrying behavior and capacity of a hybrid metal-composite joint assembly used in aircraft structures. Two numerical models were created for this purpose and compared, one that replicates the intricate spatial geometry of a honeycomb composite part and another one, equivalent to the first, that leads to a significant reduction in the complexity of the initial finite element model. This reduction had the overall effect of decreasing the number of degrees of freedom and halving the necessary time for analysis completion.

A static analysis performed on the hybrid joint models subjected to compression revealed close values for the two FE models, in terms of minimum axial strains registered in the woven glass fiber layers. The difference was more evident for the sheet placed directly under the concentrated compressive load. For the honeycomb cores, estimated maximum central displacements showed an increased value for the multilayered model compared to the single layer model, due to the more advanced internal structure of the former.

The metallic parts in the joint were evaluated both statically and under fatigue, for both numerical models. Thus, the results computed for the simplified, single layered model were similar in value to the ones obtained for the multilayered model. Axial and shear loads on the joint fasteners were in good correlation and under the predicted load carrying capacity for the investigated load case scenario. The maximum computed von Mises stress values for the metallic stiffener of the hybrid joint assembly were also comparable for the two proposed finite element models and were below the yield strength of the material. A fatigue evaluation of this member indicated, as well as in the case of the joint fasteners, the expected lifespan of the part when subjected to variable loads. The life expectancy under service was

checked, in addition, with a VBA program written for fatigue analysis, giving a close but more conservative estimate of allowable load cycles.

Given all these points, it may be stated that the single layer model may be used successfully for global types of analyses on hybrid joints, while the multilayered model should be used for more local analyses which focus on the explicit behavior of the composite material.

**Acknowledgements:** This work was supported by the POCU/993/6/13-153178 grant, co-financed by the European Social Fund through the Sectorial Operational Programme Human Capital 2014-2020.

## References

1. ARBAOUI, J., SCHMITT, Y., PIERROT, J.L., ROYER, F.X., Numerical Simulation and Experimental Bending Behavior of Multilayered Sandwich Structures, *Journal of Theoretical and Applied Mechanics*, **52**(2), 2014, 431-442.
2. BRUHN, E.F., *Analysis and Design of Flight Vehicle Structures*, Jacobs Pub., 1973.
3. NIU, M.C.Y., *Composite Airframe Structures*, Conmilit Press, 1892.
4. GALINSKA, A., Mechanical joining of fiber reinforced polymer composites to metals – a review. Part I: Bolted Joining, *Polymers*, **12**(10), 2020, 2252. <https://doi.org/10.3390/polym12102252>
5. VANDERKLOK, A., DUTTA, A., TEKALUR, A., Metal to Composite Bolted Joint Behavior Evaluated at Impact Rates of Loading, *Composite Structures*, **106**, 2013, 446-452. <https://doi.org/10.1016/j.compstruct.2013.06.004>
6. ZHANG, J., XIE, Q., XIE, Y., ZHOU, L., WANG, Z., Investigation of Mechanical Performances of Composite Bolted Joint with Local Reinforcement, *Science and Engineering of Composite Materials*, **25**(1), 2018, 75-83. <https://doi.org/10.1515/secm-2014-0371>
7. \*\*\* Ultralight Design. Available online: <https://ultralightdesign.wordpress.com/2017/10/23/material-world/> (accessed on 20.07.2023)
8. FEISTAUER, E.E., dos SANTOS, J.F., AMANCIO-FILHO, S.T., A review on direct assembly of through-the-thickness reinforced metal-polymer composite hybrid structures, *Polym. Eng. Sci.*, **59**(4), 2019, 661-674. <https://doi.org/10.1002/pen.25022>
9. GOKHALE, N.S., DESHAPANDE, S.S., BEDEKAR, S.V., THINTE, A.N., *Practical Finite Element Analysis*, Finite to infinite, 2008.
10. KARDOMATEAS, G.A., GEUBELLE, P., *Fatigue and Fracture Mechanics in Aerospace Structures*, Encyclopedia of Aerospace Engineering, 2010. <https://doi.org/10.1002/9780470686652.eae142>
11. POLLOCK, L., ABDELWAHAB, A.K., MURRAY, J., WILD, G., The Need for Aerospace Structural Monitoring: A Review of Aircraft Fatigue Accidents, *International Journal of Prognostics and Health Management*, **12**(3), 2021, 1-16. <https://doi.org/10.36001/ijphm.2021.v12i3.2368>
12. GIBSON, L.J., ASHBY, F.M., *Cellular Solids Structure and Properties-Second Edition*, Pergamon Press, 1988.
13. \*\*\* Mil Handbook, Metallic Materials and Elements for Aerospace Vehicle Structures, MIL-HDBK-5H, 1998.
14. CORMOS, R., *Evaluarea raspunsului mecanic al materialelor compozite multistrat cu miez de tip fagure solicitate la impact in domeniul vitezelor mici*, Ph.D. thesis, University Politehnica of Bucharest, 2018.
15. JU, J., SUMMERS, J.D., ZIEGERT, J.C., FADEL, G., Design of Honeycombs for Modulus and Yield Strain in Shear, *Journal of Engineering Materials and Technology*, **134**(1), 2012, 1-15. <https://doi.org/10.1115/1.4004488>
16. SEEMANN, R., *A Virtual Testing Approach for Honeycomb Sandwich Panel Joints in Aircraft Interior*, Institut für Produktentwicklung und Konstruktionstechnik, 2020.
17. \*\*\* MSC Nastran 2018 Static Analysis.
18. \*\*\* Altair, Introduction to practical aspect of composites with Altair OptiStruct.





19. CHOUDHURY, A., MONDAL, S.C., SARKAR, S., Failure analysis of laminated composite plate under hygro-thermo mechanical load and optimization, *IJAME*, **24**(3), 2019, 509-526. <https://doi.org/10.2478/ijame-2019-0032>
20. HADĂR, A., *Structuri din Compozite Stratificate, Metode, Algoritmi și Programe de Calcul*, Editura A.G.I.R., 2002.
21. HYO, S.L., JAE, R.L., YEUNG, K.K., Mechanical behavior and failure process during compressive and shear deformation of honeycomb composite at elevated temperatures, *Journal of Materials Science*, **37**, 2002, 1265-1272. <https://doi.org/10.1023/A:1014344228141>
22. SHAH, U.B., *Mechanical Properties and Failure Analysis of Cellular Core Sandwich Panel*, Master of Science in Aerospace Engineering, Blacksburg Virginia, 2017.
23. \*\*\* MSC Patran 2018 User Manual.
24. DEUTSCH, I., *Rezistența Materialelor*, Editura Didactică și Pedagogică, 1979.
25. ILIE, V., BIA, C., SOARE, M.V., *Rezistența Materialelor și Teoria Elasticității*, Editura Didactică și Pedagogică, 1983.
26. DOWNLING, N.E., *Mechanical Behavior of Materials*, Pearson edition, 2013.
27. STHEPENS, R.I., FATEMI, A., STHEPENS, R.R., FUCHS, H.O., *Metal Fatigue in Engineering Second Edition*, Jown Wiley & Sons, 2001.
28. CAMPBELL, F.C., *Fatigue and fracture understanding the basics*, ASM, 2012.
29. LEE, Y.L., BARKEY, M.E., KANG, H.T., *Metal Fatigue Analysis Handbook*, Butterworth-Heinemann, 2012. <https://doi.org/10.1016/C2010-0-66376-0>
30. LEE, Y.L., PAN, J., HATHAWAY, R.B., BARKEY, M.E., *Fatigue Testing and Analysis*, Elsevier, 2004.

---

Manuscript received: 12.09. 2023